

Article

Engineering Geological and Geophysical Investigations to Characterise the Unstable Rock Slope of the Sopus Promontory (Gozo, Malta)

Davide Pistillo ¹, Emanuele Colica ², Sebastiano D'Amico ², Daniela Farrugia ², Federico Feliziani ¹, Luciano Galone ², Roberto Iannucci ^{3,*} and Salvatore Martino ¹

- ¹ Dipartimento di Scienze della Terra & Centro di Ricerca per i Rischi Geologici CERI, Sapienza Università di Roma, P.le A. Moro 5, 00185 Roma, Italy; davide.pistillo@uniroma1.it (D.P.); federico.feliziani@uniroma1.it (F.F.); salvatore.martino@uniroma1.it (S.M.)
- ² Department of Geosciences, University of Malta, MSD2080 Msida, Malta; emanuele.colica@um.edu.mt (E.C.); sebastiano.damico@um.edu.mt (S.D.); daniela.farrugia@um.edu.mt (D.F.); luciano.galone@um.edu.mt (L.G.)
- ³ ANSFISA Agenzia Nazionale per la Sicurezza delle Ferrovie e delle Infrastrutture Stradali e Autostradali, P.le dell'Industria 20, 00144 Roma, Italy
- * Correspondence: roberto.iannucci@ansfisa.gov.it

Abstract: Different engineering geological and geophysical investigations were performed at the Sopus promontory in the island of Gozo (Malta), involved in an impressive lateral spreading process due to the superimposition of a stiff limestone (ULC) on a ductile clay (BC). The applied techniques include: traditional geological and engineering geological surveys, unmanned aerial vehicles (UAV) survey, electrical resistivity tomography (ERT) survey, ground-penetrating radar (GPR) investigations, single-station seismic ambient noise measurements, and array seismic ambient noise measurements. The integration of the obtained results allowed us to reconstruct a subsoil model of the promontory that includes features related to the local geology of the slope and to the landslide process, as well as to define a conceptual model that describes the main evolution phases of the expansion process. The presence of back-tilted rock blocks with no features of polarization of Rayleigh waves evidenced the different failure mechanism of the rigid UCL plateau at the Sopus promontory with respect to the Selmun promontory, located in the close island of Malta, where the lateral spreading due to the same geological setting tends to produce unstable rock blocks with a toppling mechanism. This result encourages further future observations and analyses of this topic.

Keywords: lateral spreading; UAV; ERT; GPR; HVNR; ESAC; Malta; Gozo



Citation: Pistillo, D.; Colica, E.; D'Amico, S.; Farrugia, D.; Feliziani, F.; Galone, L.; Iannucci, R.; Martino, S. Engineering Geological and Geophysical Investigations to Characterise the Unstable Rock Slope of the Sopus Promontory (Gozo, Malta). *Geosciences* **2024**, *14*, 39. <https://doi.org/10.3390/geosciences14020039>

Academic Editors: Piotr Migoń and Jesus Martinez-Frias

Received: 31 December 2023
Revised: 27 January 2024
Accepted: 31 January 2024
Published: 1 February 2024



Copyright: © 2024 by the authors. Licensee MDPI, Basel, Switzerland. This article is an open access article distributed under the terms and conditions of the Creative Commons Attribution (CC BY) license (<https://creativecommons.org/licenses/by/4.0/>).

1. Introduction

Lateral spreading (sensu Cruden & Varnes [1], Hungr et al. [2]) represents a slowly evolving landslide process that can be activated by the juxtaposition of lithologies with rigid behaviour overlying lithologies with a ductile one. Their manifestation leads to block dislodging caused by large open fractures up to trenches and to their mutual distancing. The isolated blocks generate wall instability which, in turn, gives rise to more localised detachments from the rock walls, such as collapses or overturning, commonly causing huge accumulations of debris at the base of the slopes.

From a rheological point of view, these processes evolve with the gradual damage of the masses involved, i.e., they cause the progressive jointing and fragmentation of the same, which is accompanied by a loss of mechanical resistance and stiffness properties [3]. This preparatory process often results in an acceleration of the deformations driven by an increase in the stiffness contrast that controls them. In addition, polarization effects, related to surface waves that cause the focusing of ground motion along certain directions, can also be detected. Such an effect generally occurs along a normal direction with respect to the main joints which bound the rock blocks, making them more prone to detachment [4,5].

Several studies demonstrated how the damage associated with rock mass deformations in systems involved in lateral spreading is visible through geophysical investigations which reveal both the increase in fracturing of the stiff rock involved and the softening of the underlying ductile material. This, for example, translates into an increase in seismic impedance contrast, which can lead to an intensification of local seismic amplification, in turn causing more intense destabilising actions caused by gravity [6].

In relation to the above, the lateral spreading processes can be defined as “viscosity driven”, i.e., driven by creep which affects the ductile lithologies present at the base of the stone plateaus with more rigid behaviour [7,8]. The slow evolution, however, does not prevent these processes from causing high risk conditions where they tend to threaten anthropic infrastructures, buildings, or even monuments, which can be involved in the retreat of the surrounding unstable slopes subject to lateral spreading precisely because they have been built for several centuries.

Furthermore, lateral spread is an important proxy for the climatic evolution linked to the retreat of the coasts, as it is a combination of eustatism and regional uplift of geodynamic origin. In this sense, the slopes surrounding the reliefs involved in these landslide processes can gradually retreat until they are completely isolated from the action of the sea waves, evolving from the sea cliffs to inland slopes.

The slow evolution of lateral spreading processes commonly makes them poorly, if at all, visible to remote sensing techniques (such as satellite interferometry), since strain rates can be significantly below the sensitivity levels of these detection systems. In this sense, the application of integrated engineering geological and geophysical techniques represents a fruitful strategy for the reconstruction of the instability mechanisms linked to lateral expansions, as well as for monitoring their evolution, if, when repeated over time, they reveal perceptible changes in the mechanical properties of the rocks involved.

The islands of Malta and Gozo are both very prone to gravity-induced instabilities connected to lateral spreading [9], given a strongly predisposing geological setting due to the overlapping of stiff calcarenites (Upper Coralline Limestone) above ductile clays (Blue Clays). In the entire western portion of the island of Malta, this geological setting is clearly visible with a geological limit a few metres or tens of metres above the current sea level. In relation to these different predisposing conditions, on the island of Gozo, the ongoing lateral spreading is still strongly interacting with the marine wave motion and is subjected to its erosive and destabilising action. On the other hand, on the island of Malta, except for some cases which mostly involve the south-western coast of the island, the marine action is widely distanced from the scarps which delimit the lateral expansion processes which, therefore, continue their evolution under the action of gravity and atmospheric agents [10].

The present study focused on the Söpu promontory, located north of the town of Nadur, on the north-eastern sector of the island of Gozo, which hosts an impressive process of lateral spreading whose evolution generated an extensive field of coastal blocks that, to this day, come to interact with the sea and its erosive activity. The progressive pattern related to the rock mass damaging is observed in the Miocene calcarenite plateau, i.e., with a decreasing joint frequency from the edge of the cliff towards the inland areas, makes the Söpu promontory site an excellent laboratory for the application of integrated engineering geological and geophysical investigation techniques aimed at detecting evidence of activity due to landslides of the type considered here. More specifically, as will be described in detail in the following paragraphs, several techniques were applied: geological and engineering geological surveys to reconstruct the subsoil model and the joint network; photogrammetric surveys with a drone to obtain a high-resolution digital terrain model; single-station seismic ambient noise investigations to evaluate the resonances related to the seismic impedance contrasts generated by the juxtaposition of the lithologies attributable to the local stratigraphic succession and the vibrational behaviour of the unstable zones; array seismic ambient noise measurements to derive the local seismostratigraphy and correlate it with the geological setting; and ground-penetrating radar investigations to highlight the presence of discontinuities and their persistence throughout and inside the summit stone

plateau, with the aim of relating these properties to their genesis. It is, in fact, conceivable that, as a result of a lateral spreading, the joints tend to propagate from below (i.e., from the rigid/ductile contact) upwards, precisely in relation to the fact that the driving force of the deformation process is the vertical juxtaposition of lithologies with different stiffness which, therefore, responds to the stresses due to the lithostatic load with significantly different levels of effort. Consequently, the latter concentrates in the rigid plateau along the contact with the ductile medium, causing it to fracture with a gradual propagation towards the surface.

Such a genesis of cracks induced by the gravity-induced process is, in turn, predisposed to processes of wall detachment by sliding (as evidenced by back-tilted blocks) or by toppling, when the high-angle joints isolate stone columns developing along the perimeter of the cliffs.

Based on the above-reported considerations, the application of the integrated techniques at the Sopus promontory site also aimed to represent their suitability, in order to deduce a more constrained diagnosis on the mechanism of evolution of the instability processes under consideration.

2. Geological and Geomorphological Setting

Together with Malta and Comino, the island of Gozo belongs to the Maltese archipelago, a group of islands located in the central Mediterranean Sea, about 90 km south of Sicily and 290 km north-east of Tunisia. The islands are situated in the northern African Plate in correspondence with the so-called Malta Graben [11], an important part of the threshold separating the Western and Eastern Mediterranean basins [12].

The Maltese archipelago is crossed by two fault systems: the WSW–ENE-oriented “Great Fault” system and the NW–SE-trending system [13–15]. The first one controls a horst and graben structure [16], while the second conditions the NE and SE coasts’ orientation. The Maltese islands represent the emergent part of a shallow-water marine succession that are composed of Late Oligocene (Chattian) to Late Miocene (Messinian) rocks mostly composed of limestones and marls [13]. Five lithostratigraphic units form the outcropping sequence [17–20] (Figure 1). The oldest is represented by the Lower Coralline Limestone Formation (LCL) (Chattian) of pale grey, hard and shallow marine biomicrites and biosparites around 140 m thick. Younger formations follow, starting with: (i) the Globigerina Limestone Formation (GL) (Aquitainian–Langhian), a yellowish, fine-grained, planktonic foraminifera limestone; (ii) the Blue-Clay Formation (BC) (Serravallian–Tortonian), which consists of grey soft marls; (iii) the Greensand Formation (Tortonian), which is a brown and greenish glauconite-rich 1–11 m thick member; and (iv) the Upper Coralline Limestone Formation (UCL) (Tortonian–Messinian), which is broadly similar to the LCL. The geological formations lie almost horizontally across all the islands, showing a 5° tilting towards NE due to the upwarping of the NE shoulder of the Malta Graben, part of the Pantelleria Rift System and on which the islands are settled [16].

The island of Gozo is characterised by varied landscapes, mainly controlled by litho-structural, marine, gravitational, karst, and fluvial morphogenetic factors [21,22]. The different resistance to erosion of the above-described lithostratigraphic units controls the evolution of several landforms, such as the numerous landslides distributed along the coastline. This is the case of the superimposition of brittle limestone plateaus (i.e., UCL) over clayey terrains (i.e., BC), which favour the fracturing of the overhanging units and the development of lateral spreading phenomena [23] which tend to evolve into block sliding and rock topple and falls [4,5,9,21,24].

Soldati et al. [25] hypothesised that the lateral spreading landslide system of the Maltese archipelago developed during a sea-level low-stand and was subsequently submerged by post-glacial sea-level rise. Exposure dating results demonstrate indeed that some of the oldest dated block detachments occurred in a subaerial environment at ca. 21 kyrs when the sea level was about 130 m lower than at present. For this reason, most of the landforms now observable on the seafloor are related to subaerial processes.

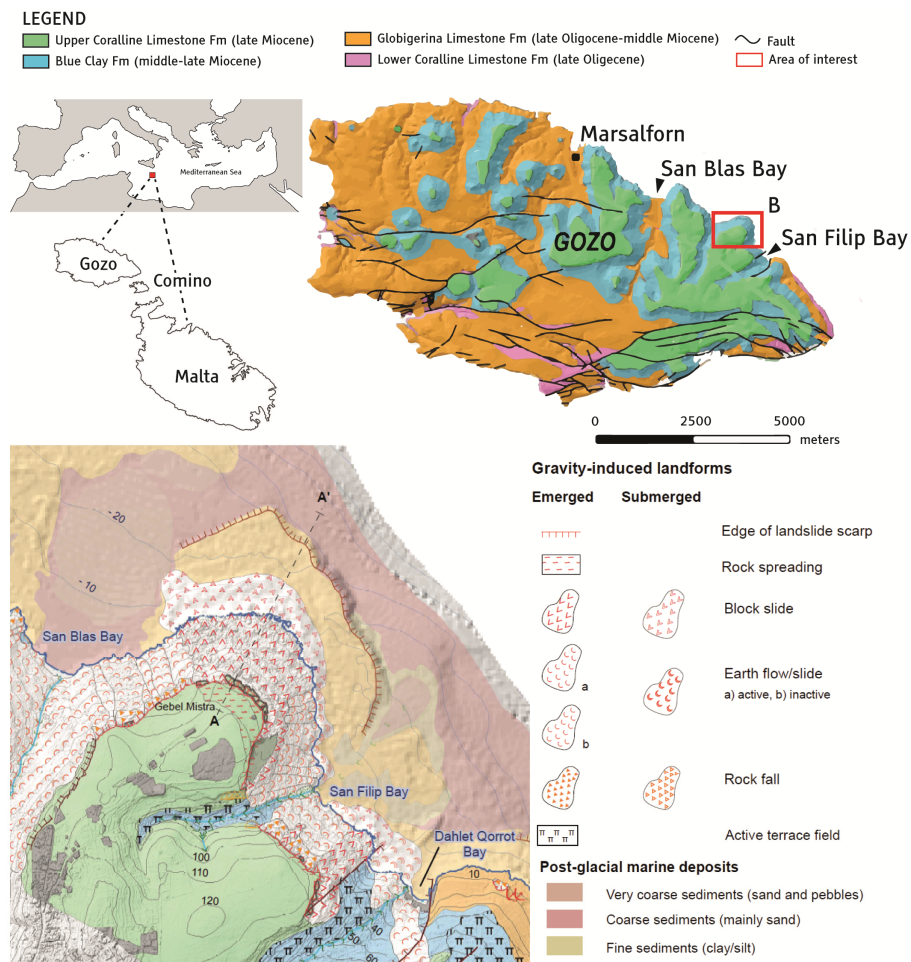


Figure 1. Localisation of the Maltese archipelago in the Mediterranean Sea and geological map of the island of Gozo by the Oil Exploration Directorate [17] (**top**) and geomorphological map of the Sopu promontory (**bottom**) (from Prampolini et al. [21], reproduced with the permission of Taylor & Francis Ltd., Journal of Maps 2018 <https://www.tandfonline.com> accessed on 27 January 2024).

The Sopu promontory was chosen as a case study because of its involvement in an impressive lateral spreading process that is threatening the cultural heritage site of the homonymous watchtower. The promontory is located along the east coast of the island of Gozo, between the San Blas and San Filip Bays, and it is bounded by a scree-type beach sensu. The area stands on the hanging wall sector of the South Gozo Fault, a normal fault belonging to the Great Fault system and crossing the southern margin of Gozo. This tectonic lineament is responsible for the uplift of the Oligo-Miocene succession, evidenced by the GL and LCL outcrops above the sea level in the southern sector of the island of Gozo.

The stratigraphic succession of the Sopu Promontory is composed of about 50 m of the UCL Formation, which occupies the topographic high of the plateau and the underlying BL and GL formations for the remaining portion of the slope. All the formations rarely outcrop along the slope because of the presence of a significant slope debris deposit resulting from the UCL plateau disintegration. The same slope deposit also covers the contact between BL and GL units, which is supposed to be located more or less in correspondence with the shoreline. The calcareous plateau is desiccated by several joints progressively more open-moving towards the perimeter of the highland. The parietal portions of the plateau are thus visibly disjointed from the overleaf plateau due to the ongoing lateral spreading process. This latter favours the detachment of single rock blocks by typical gravity-induced instability mechanisms, i.e., planar sliding, wedge sliding, toppling, and falling [26]. The

resulting landslide process can be defined as complex, according to Cruden & Varnes [1] and Hutchinson [27].

In the stretch of sea in front of the Sopu promontory, Prampolini et al. [21] identified offshore an NW–SE-oriented escarpment that has been interpreted as a structural origin; it acted as a former sea cliff around 10 kyrs ago when the sea level was about 30 m lower than today [28].

3. Site Investigations

Between 2020 and 2021, several engineering geological and geophysical investigations were performed at the Sopu promontory to reconstruct the geological setting of the unstable slope and the joint network that characterises it, as well as to provide a conceptual model of the gravity-induced process of evolution. In particular, the following techniques were applied at the promontory (Figure 2):

- Geological and engineering geological surveys;
- Unmanned aerial vehicles (UAV) survey;
- Electrical resistivity tomography (ERT) survey;
- Ground-penetrating radar (GPR) investigations;
- Single-station seismic ambient noise measurements;
- Array seismic ambient noise measurements.

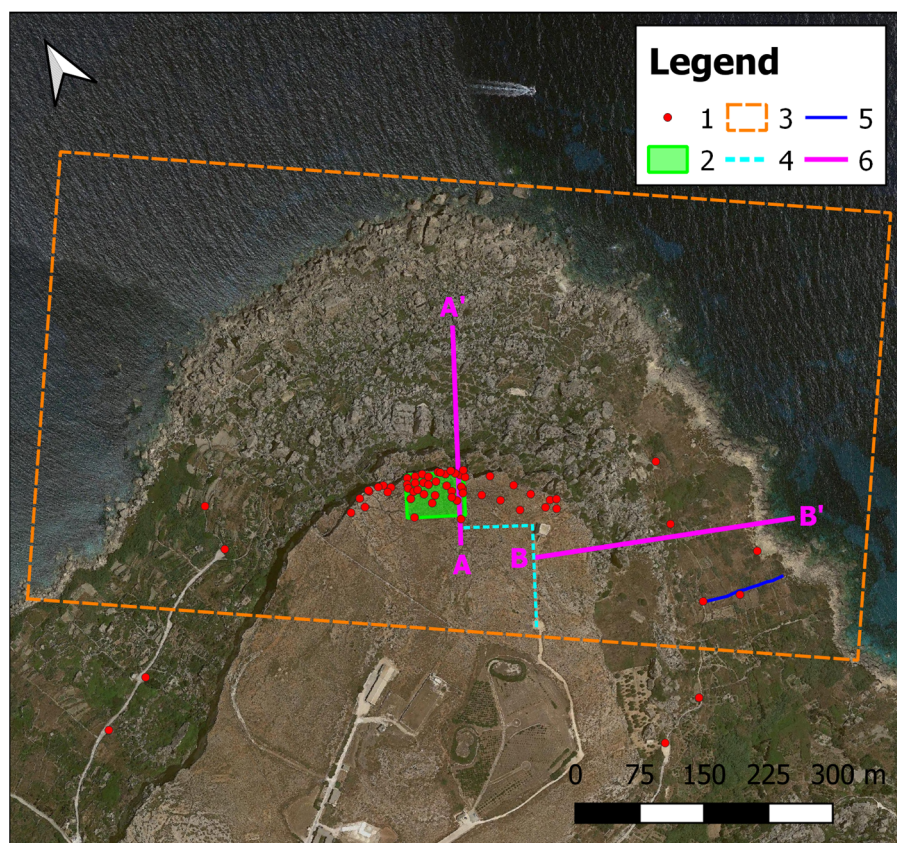


Figure 2. Satellite view showing the investigations performed at the Sopu promontory. Legend: (1) single-station seismic ambient noise measurements; (2) GPR surveys; (3) UAV surveys; (4) ESAC array; (5) ERT survey; and (6) cross-sections track (with ID).

3.1. Engineering Geological Surveys

Accurate engineering geological surveys were carried out in the Sopu Promontory in order to detail the geological setting of the area and to conceptualise the engineering geological model of the coastal slope. A dense network of fractures dissects the carbona-

ceous plateau composing the UCL Formation. In situ and remote analyses were carried out to precisely detail the geomechanical features of the joint sets. In these terms, the direct fracture characterisations carried out on the plateau are low since a dense vegetation cover overlays almost the entire highland. The other recognized joints have been detected thanks to UAV survey techniques using a procedure that will be illustrated in the following paragraph.

Each fracture was characterised according to the ISRM standard [29], defining the: attitude (dip direction and dip), spacing, persistence, aperture, and filling. Apart from the NW-dipping bedding J0 (352/3), two main sub-vertical joint sets have been recognized: J1 (5/85) which strikes more or less parallel to the plateau perimeter, and the conjugate set J2 (94/85) (Figure 3). The fracture aperture gradually increases when moving toward the edge of the plateau, reaching dimensions in the order of 1 m. The parietal section of the plateau is rich in ground depressions genetically linked with karst processes and partially or totally filled with red soils. The rock blocks disjointed by the lateral spreading process located close to the edge of the highland are characterised by back-tilted summit surfaces that tend to be increasingly rotated by the secondary gravitational processes.

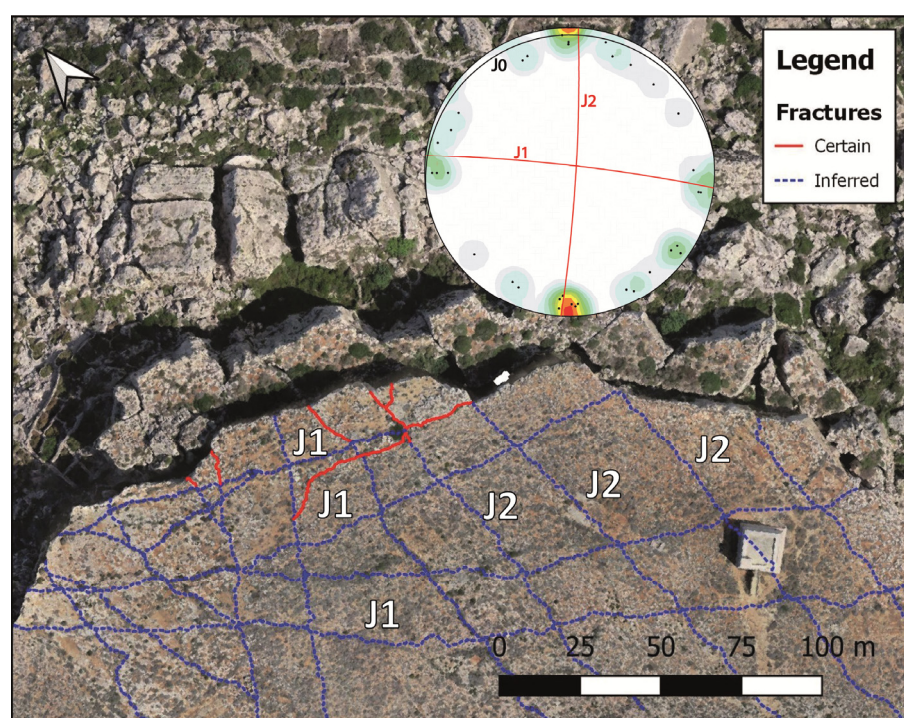


Figure 3. Orthophoto showing the distribution of joints on the UCL plateau and synthetic representation of the joint dips (dots) in the Schmidt stereonet with identified the two main joint sets (red lines) and the bedding (black line).

As for the characterization of the rock matrix, it is in agreement with what was already found by Iannucci et al. [4] for the UCL Formation at the Selmun promontory in the close island of Malta.

3.2. UAV Surveys

The coastal plateau in question was surveyed using UAV photogrammetric acquisition, meticulously planned and executed to fully capture the topographic details of the cliff and slope (Figure 2). Unmanned Aerial Vehicle (UAV) photogrammetry is a powerful tool for generating high-resolution 3D models of various landscapes, including coastal scenery [30–32] and other landforms [33].

For this investigation, the DJI Phantom 4Pro UAV, equipped with a 20 Megapixel high-resolution camera with a 1" Exmor R CMOS image sensor [34] capable of capturing detailed

images with exceptional clarity and precision, was used. Flight planning was conducted to ensure optimal area coverage with 80% longitudinal and 75% lateral overlap, considering various altitudes and angles to facilitate the generation of a complete dataset for subsequent analysis. The investigation was performed under nadiral sun conditions, taking advantage of favourable lighting conditions to maximise image quality and minimise shadows that could potentially distort the resulting dataset. The drone followed pre-programmed flight paths, capturing over 2000 high-resolution images, meticulously covering the diverse terrain of the coastal plateau. These images were georeferenced with precise position coordinates thanks to the use of 20 ground control points measured with Topcon Hiper HR DGNS receivers in Base + Rover configuration, capable of horizontal accuracy of $3 \text{ mm} \pm 0.1$ part per million and vertical accuracy of $3.5 \text{ mm} \pm 0.4$ part per million. This approach allowed the creation of a robust dataset essential for photogrammetric processing, ensuring an accurate spatial reference for subsequent processing steps.

After the flight, the collected images were processed using Agisoft Metashape photogrammetry software (Professional Edition, Version 2.0) [35]. The initial phase involved aligning and merging the images to reconstruct the camera grip position and create a sparse point cloud. Advanced SfM (structure from motion) algorithms were used to correct distortions and align images. This reconstruction process involved identifying key landmarks within the images, triangulating their locations, and creating a detailed 3D point cloud representing the surface topography of the plateau. A high-resolution digital surface model (DSM) was generated from the dense 3D point cloud data, capturing the surface irregularities made up of the plateau itself and the collapsed blocks above the BC layer. The subsequent processing involved the extraction of the orthomosaic, obtained from the aligned and corrected images, which offer a georeferenced and uniform representation of the investigated area. This orthomosaic served as a valuable tool for visual inspection and precise measurements of the affected area.

Finally, the 3D model was reconstructed with mesh and texture, which provides a detailed and interactive representation of the topography of the coastal plateau. This model facilitates in-depth analyses, such as joint characterization and volumetric calculations, and helps to better understand the erosion processes affecting the area.

3.3. GPR Survey

In an area north of the promontory of Sopus, within a polygon measuring 68×50 m (Figure 2), GPR data were collected along 69 parallel profiles set 1 m apart using the data acquisition system SUBECHO SE-70 aerial antenna, operating in the range of 20–140 MHz, with a central frequency of 80 MHz and a two-way travel time (TWTT) range of 500 ns. Data were processed using Prism2 software (<https://www.radsys.lv/en/products-soft/prism2.5+software/> accessed on 27 January 2024) using the following workflow:

- Zero-time adjustment;
- Background removal;
- Band-pass filters;
- Gain function adjustment;
- Time to depth conversion.

We implemented zero-time adjustment to align zero-time with zero-depth, background removal techniques to eliminate noise, along with band-pass and horizontal high-pass filters to enhance the signal-to-noise ratio. Time-varying gains were employed to counteract attenuation, spherical divergence, and radio signal scattering. Since the survey site is almost flat, the effect of topography on the geometry of the reflectors is insignificant, so no topographic correction was applied.

For limestone rock, the dielectric constant may vary from 7 to 8 [36]. For the present study, we considered the dielectric constant of 8 that provides a radar velocity of 0.106 m/ns. The maximum depth reached was about 10 m. In the B-scan analysis, several reflectors were evident between 2 and 8 m depth (Figure 4), and the various anomalies detected were reported in CAD and superimposed on the fractures visible from the surface and

those deduced from the analysis of the orthomosaic (Figure 5). By observing the anomalies visible from the ground-penetrating radar data in plain view, it was possible to notice alignments and deduce the path of fractures that are buried and not visible from the surface. Among the GPR anomalies, there is also a good overlap with the fractures inferred from the orthomosaic and those exposed on the surface.

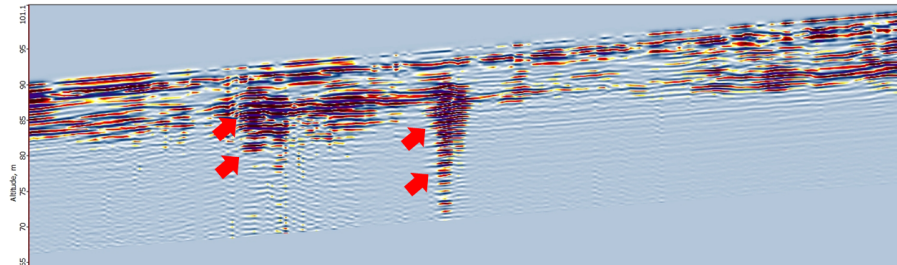


Figure 4. Example of a B-scan in which the patterns of fractures in the rock are visible (red arrows).

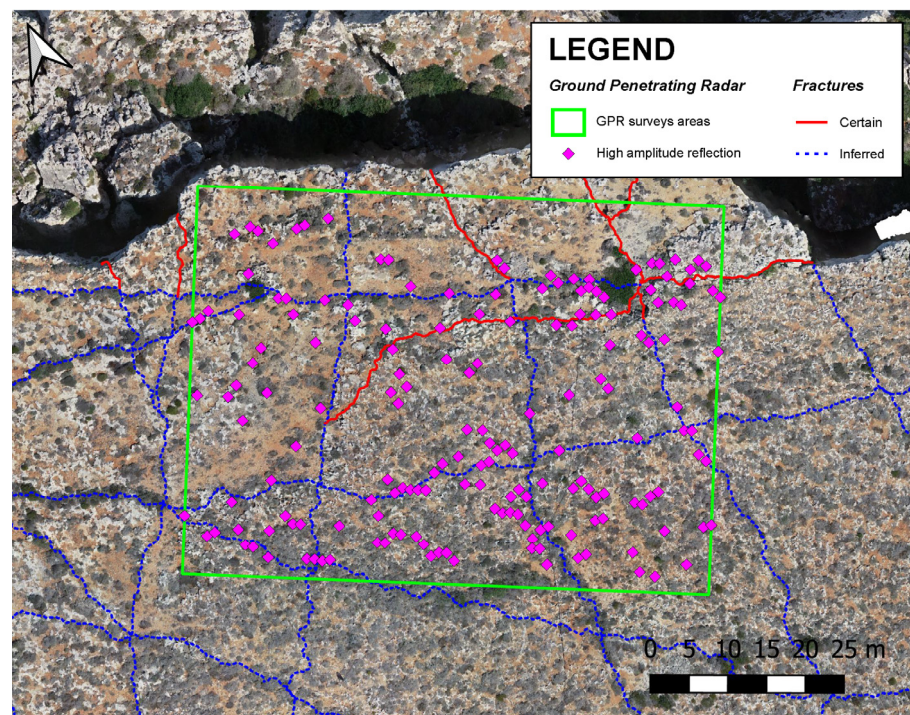


Figure 5. The figure shows the green polygon superimposed on the orthomosaic, and represents the ground-penetrating radar survey area. The purple square symbols indicate the points where anomalies were identified in the B-scans at depths between 2 and 8 m.

3.4. ERT Surveys

In June 2022, we conducted an ERT investigation on the eastern slope of the Sopus promontory (Figure 2). The array was set up on the BC Formation, which occasionally exhibits signs of disturbance and is at times covered by vegetation and limestone clasts originating from the UCL that culminate on the Sopus promontory (Figure 6).

For this investigation, we deployed a set of 32 electrodes with a 3 m spacing between them, using a multichannel digital resistivity m ELECTRA (Moho srl, Venezia, Italy). To ensure the proper electrode coupling and prevent potential issues, impedance tests were carried out, with results consistently below 1000 ohms in all cases and often below 500 ohms, confirming optimal electrode–soil contact conditions.

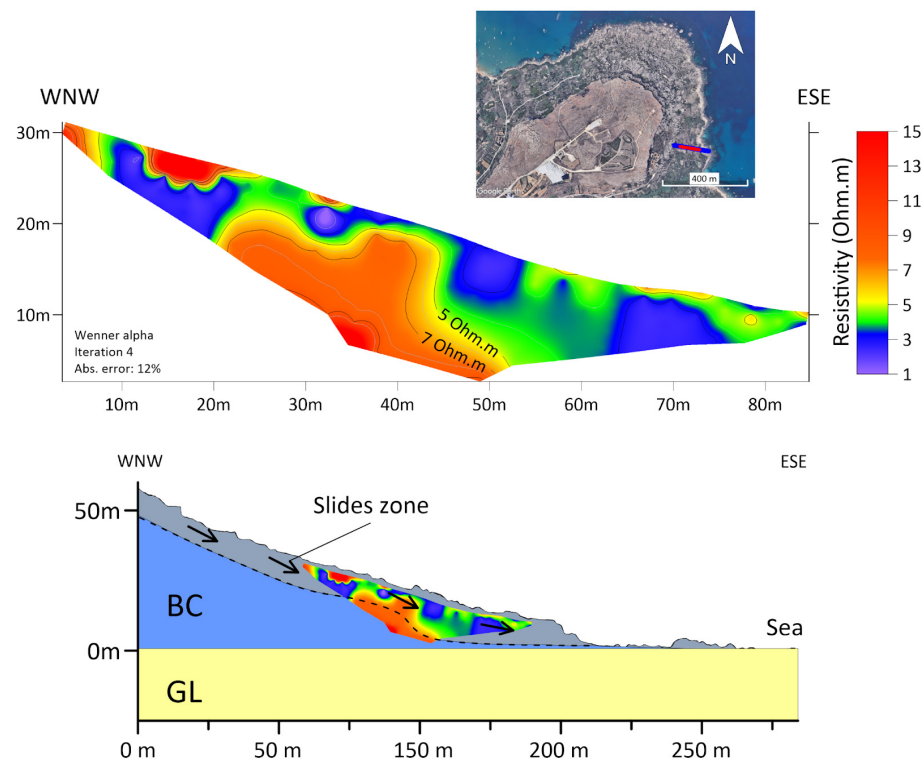


Figure 6. ERT results. The red line in the satellite image represents the ERT position, and the blue line represents the geological cross-section of the bottom panel. A high-gradient resistivity zone is related to the lower limit of a relatively plastic zone, represented by the dashed line in the geological cross-section.

Data acquisition was performed using the Wenner Alpha array. The electrode positions, including elevation, were acquired using a centimetre-accurate GNSS. The inversion of apparent resistivity data obtained in the field was conducted using Res2inv software version 4.8.10, following standard procedure [37–39], reaching an absolute error of 12% after 4 iterations.

The ERT model obtained reveals generally low resistivity values, ranging from 1 to 15 Ohm.m. These values align with the typically conductive characteristics of clays, as expected for the BC Formation. In the shallow section of the tomography, notably low resistivity values are observed, often below 5 Ohm.m, with occasional exceptions in the form of local high-resistivity anomalies, particularly at $m X = 15$.

In the central area of the tomography, corresponding from $m X = 20$ to $X = 50$, the model reaches greater depths, with a maximum thickness of about 15 m. At a depth of approximately 7 m from the surface, a positive gradient is observed towards deeper regions, where the maximum resistivity values are attained.

Our interpretation suggests that the less resistive superficial layer corresponds to the BC with high moisture content, along with slope clastic deposits interspersed within a clay matrix composed of BC material. In some locations, these clasts may have metric dimensions, locally increasing resistivity values. We speculate that this layer could exhibit relatively higher plasticity and act as a slide zone, with a thickness of approximately 7 to 10 m. This plastic layer may extend across the entire slope and be responsible for the downslope transport of small- and medium-dimension clastic material.

In the deeper sections of the tomography, the increase in resistivity values may indicate a region with lower moisture content, potentially less plastic, and geotechnically more stable.

3.5. HVNR and Polarization Analysis

Considering the reconstructed engineering geological model of the promontory and the reconstructed joint network, 65 seismic ambient noise measurements were performed in a single-station configuration. The measurements were distributed on the UCL plateau, covering areas with and without joints, and the BC slope (Figure 2), to assess the site resonance frequencies of the different lithotechnical units outcropping, as well as to evaluate the vibrational behaviour of the identified rock blocks. The measurements were performed using three different instruments: (i) SL06 24-bit digitisers with built-in SS20 2.0-Hz three-component velocimeter from SARA Electronic Instruments set to a sampling frequency of 250 Hz; (ii) Tromino 3-component portable seismographs from Micromed set to a 256 Hz sampling frequency; (iii) Geobit with 200 Hz sampling frequency. Seismic ambient noise was recorded between 45 min and 1 h in each measurement site.

The measurements were analysed according to the Horizontal-to-Vertical Spectral Noise Ratio (HVNR) technique. The HVNR analysis was proposed by Nogoshi & Igarashi [40,41] and implemented by Nakamura [42] to define the fundamental frequency (f_0) of a site characterised by a stratigraphy with a marked impedance contrast, such as a soft soil on a stiff bedrock [43,44], even if it was widely used in non-standard conditions to analyse the changes occurring in the seismic waves due to particular geological, geomorphological, and geomechanical settings, such as unstable rock blocks [4,5,45–47]. The HVNR analysis was performed using Geopsy software (version 3.5.2) [48] on the record of each measurement according to the following main steps: the Fast Fourier Transform (FFT) was computed on non-overlapping time windows of 40 s with 5% cosine taper for the 3 motion components (i.e., North–South, East–West, and Up–Down); the smoothing function by Konno & Ohmachi [49] was applied on the FFT spectra computed for each time window; the HVNR function was computed for each time window as the ratio between the quadratic mean of the 2 horizontal (H) FFT spectra and the vertical (V) FFT spectrum; the mean HVNR function of the measurement was obtained by averaging the HVNR computed on the single time windows.

The seismic ambient noise records were also analysed in terms of the polarization of the particle motion [50] using the WAVEPOL code developed by Burjánek et al. [51,52], based on the hypothesis that a wavefield within a jointed rock mass due to ongoing deformations is dominated by normal mode vibration rather than horizontal propagation of seismic waves. It was already applied to evaluate the vibrational behaviour of unstable rock masses. The WAVEPOL code applies the Continuous Wavelet Transform (CWT) for obtaining the particle motion at each time-frequency pair as a 3D ellipse, where the ellipticity is the ratio between the semi-minor axis and the semi-major axis of the ellipse (i.e., 1 for circular motion and 0 for linear motion), and the polarization is indicated by 2 angle values: a strike value, corresponding to the azimuth of the semi-major axis projected from North to the horizontal plane, and a value for the dip angle of the semi-major axis with respect to the horizontal plane.

All the measurements performed on the UCL plateau present HVSr functions with a main resonance peak at 1.1–1.2 Hz, followed by a sharp dip below 1.0 (Figure 7, left and middle panel). This peak can be associated with the fundamental frequency of the site (f_0) that can be observed where the UCL-BC-GL sedimentary sequence outcrops on the Maltese archipelago [4,5,45–47,53–57], and was attributed to the presence of the low-velocity clay layer between the two higher velocity limestone layers [46]. This 1.1–1.2 HVSr peak is associated with “eye-shape” Fourier amplitude spectra [58], i.e., an increase of the horizontal Fourier spectra and a decrease of the vertical Fourier spectrum, and no marked polarization, confirming that it is related to a 1D resonance effect due to the local stratigraphical setting. Also, the HVSr functions obtained from the stations located on the BC slope (Figure 7, right panel) show a main peak that can be associated with the fundamental frequency of the site (f_0). This HVNR peak is due to a resonance in the BC layer, and its value varies between 1.5 and 6.0 Hz (Figure 8), based on the location along the slope and, therefore, the thickness of the BC layer itself.

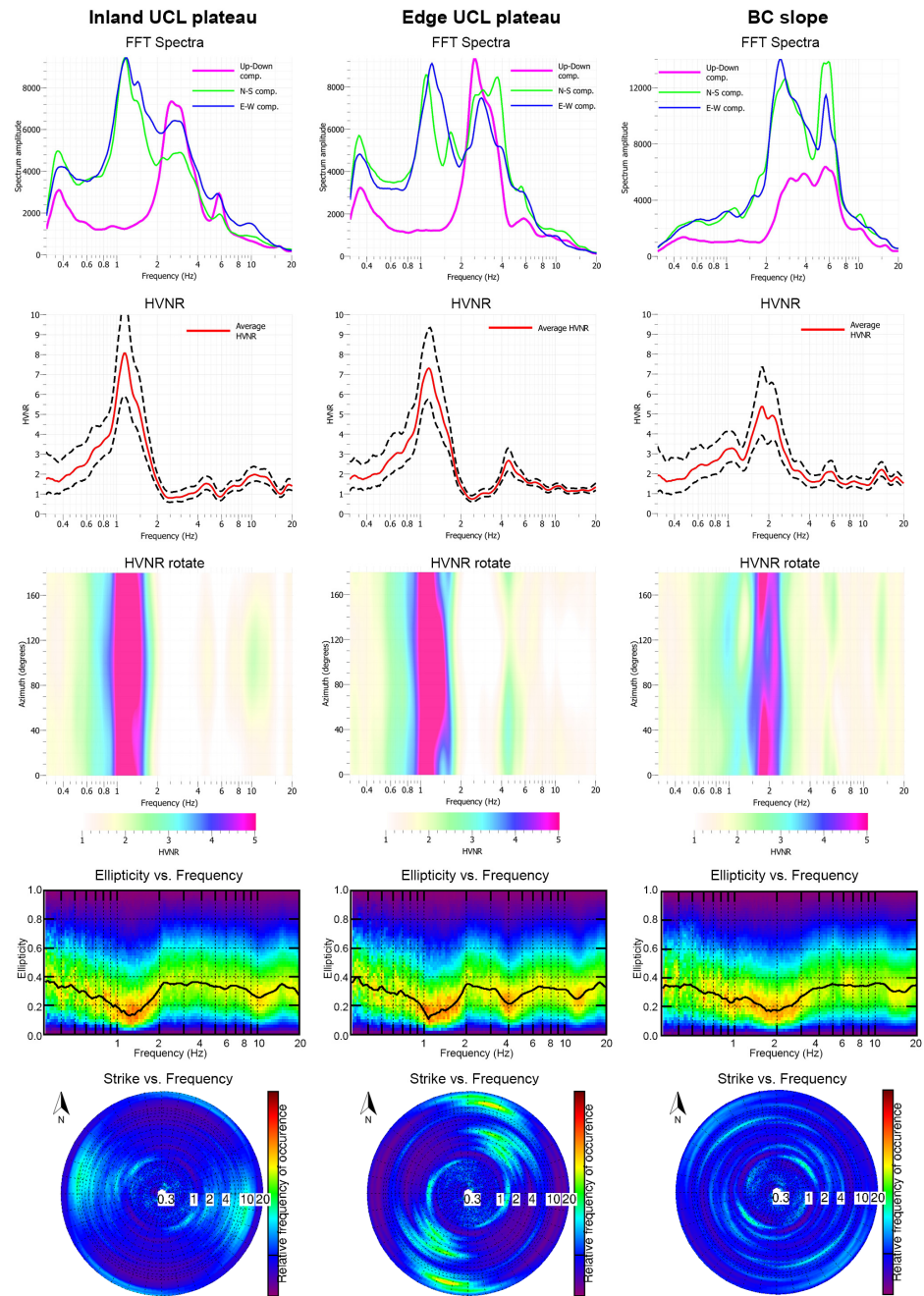


Figure 7. Examples of FFT spectra, HVNR function (the dashed black lines show the standard deviation of the curve), HVNR rotate, ellipticity diagram, and polar strike plot (same palette colour for the relative frequency of occurrence) obtained on the non-fractured UCL plateau (**left**), fractured UCL plateau (**middle**), and BC slope (**right**).

In addition, the HVNR functions obtained on the UCL edge plateau reveal an additional significant peak (f_1) at a frequency between 3.0 and 8.0 Hz (Figure 7, middle panel) that presents a weak polarization in the HVNR rotate analysis. This additional HVNR peak (Figure 9) presents an HVNR polarization roughly orthogonal to the edge plateau direction. The WAVEPOL analysis does not show features of linearity, nor polarization of the particle motion, as evidenced by the ellipticity and polarization plots (Figure 7, middle panel). The measurements performed in the inland part of the UCL plateau and on the BC slope do not reveal significant additional peaks in the HVNR functions.

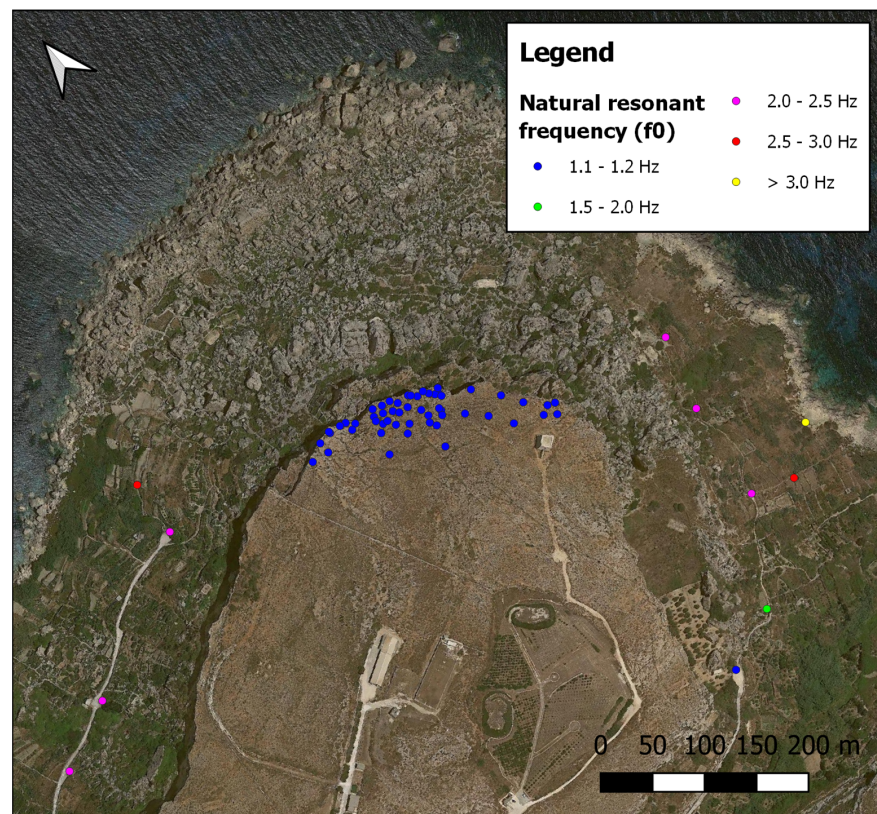


Figure 8. Satellite view showing the site natural resonant frequency (f_0) from the HVNR analysis.

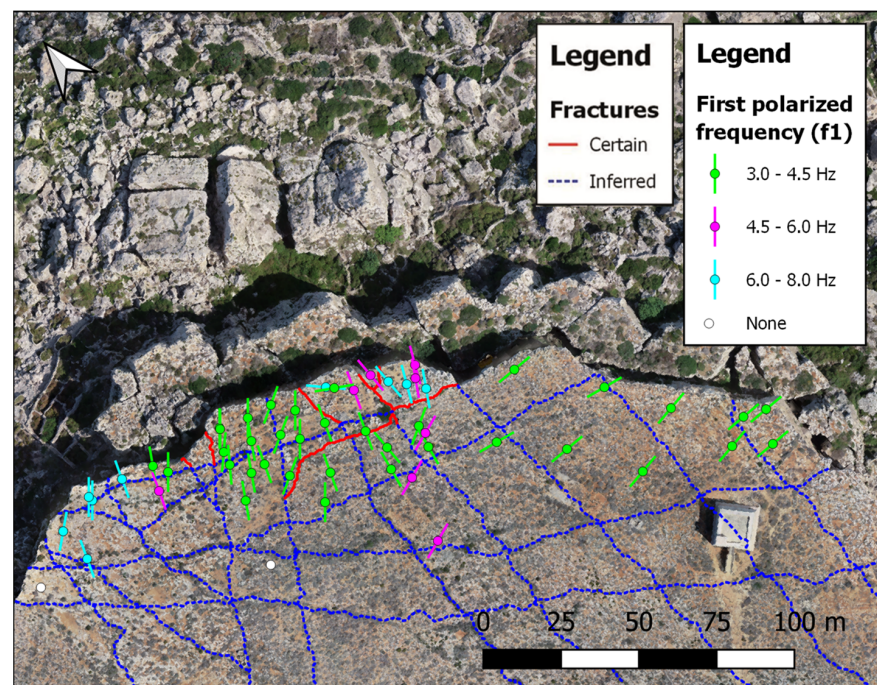


Figure 9. Orthophoto showing the first polarized frequency (f_1) from the HVNR rotate analysis.

3.6. ESAC Analysis

Seismic array measurements have been taken on the UCL plateau (Figure 2) by acquiring ambient noise using a Micromed SoilSpy Rosina™ seismic digital acquisition system equipped with 4.5 Hz vertical geophones. A total of 42 geophones were deployed in an

L-shaped arrangement with a regular interstation spacing of 5 m. The recordings, each lasting 20 min, were processed using the ESAC technique (for details of the method, refer to Farrugia et al. [55] and references therein). Given the use of only vertical sensors, the detected signals were interpreted as plane Rayleigh waves in their fundamental and higher propagation modes [59].

In this study, we estimated a 1-D V_s profile by jointly inverting H/V and the effective dispersion curves using the Genetic Algorithm (GA) approach [60,61]. The joint inversion procedure leveraged two datasets sensitive to different properties, enabling the extraction of information about the deeper part of the profile not captured in the low-frequency segment of the dispersion curve (e.g., [62–65]). Several studies (e.g., [53,66–68]) have employed the joint inversion technique, consistently yielding reliable results closer to available geotechnical data than those obtained through conventional inversion procedures. The GA, an iterative procedure concentrating exploration in more promising areas within a research space [55,68], was utilised. Starting with 100 randomly generated models, a subset of the best models was chosen, and genetic operators (cross-over, mutation, and elite selection) were applied to simulate genetic selection, creating a second generation of models. This process was iterated 150 times. Ten separate inversions were conducted, and the best-fitting profile for each was saved. The final result was selected based on the minimum misfit value, where synthetic H/V and effective dispersion curves best matched the experimental ones, in accordance with established measures, among all 10 inversions. The other top results served to estimate the inversion result variability and robustness.

Figure 10 shows the results of these analyses, the derived V_s profile, and the geological interpretation obtained using the data available for the site, from the top to the bottom: a UCL layer with a thickness of 45–50 m, with V_s values of about 750 m/s in the first 5–10 m and higher than 900 m/s in the underlying part; a BC layer from 45–50 m to about 110–120 m, with V_s values of about 450 m/s in the first 25–30 m and about 600 m/s in the underlying part; a GL layer from about 110–120 m with a V_s value of about 1400 m/s.

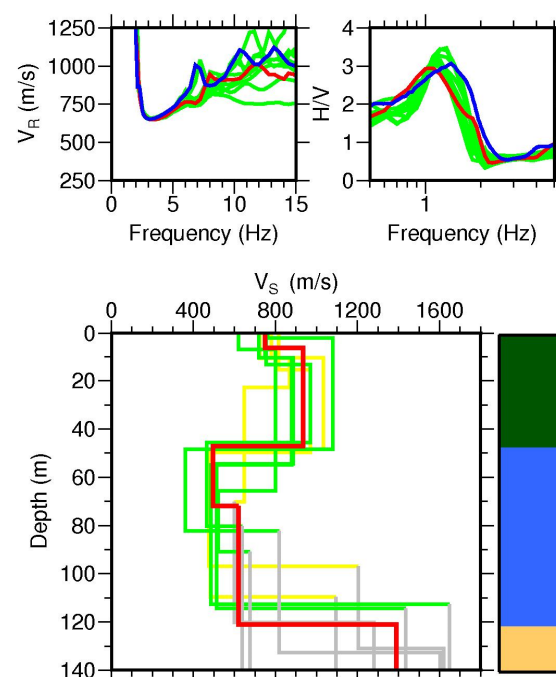


Figure 10. The joint inversion results and stratigraphic interpretation (**lower panel**). Top panel shows the effective dispersion and H/V curves: in red, the best model; in grey, green, and yellow, the models with higher misfit values; in blue, the experimental data.

4. Results and Discussion

The results obtained by the engineering geological and geophysical investigations were integrated to reconstruct a subsoil model of the Sopu promontory that included features related to the local geology of the slope as well as to the landslide process (Figure 11). In particular, this model allowed to:

- Constrain the depth of the UCL-BC and BC-GL geological contacts;
- Define the thickness variation of the BC Formation along the slope;
- Characterise the debris, UCL blocks, and softened BC along the slope;
- Characterise the joint systems existing in the UCL;
- Evaluate the vibrational behaviour of the unstable UCL blocks.

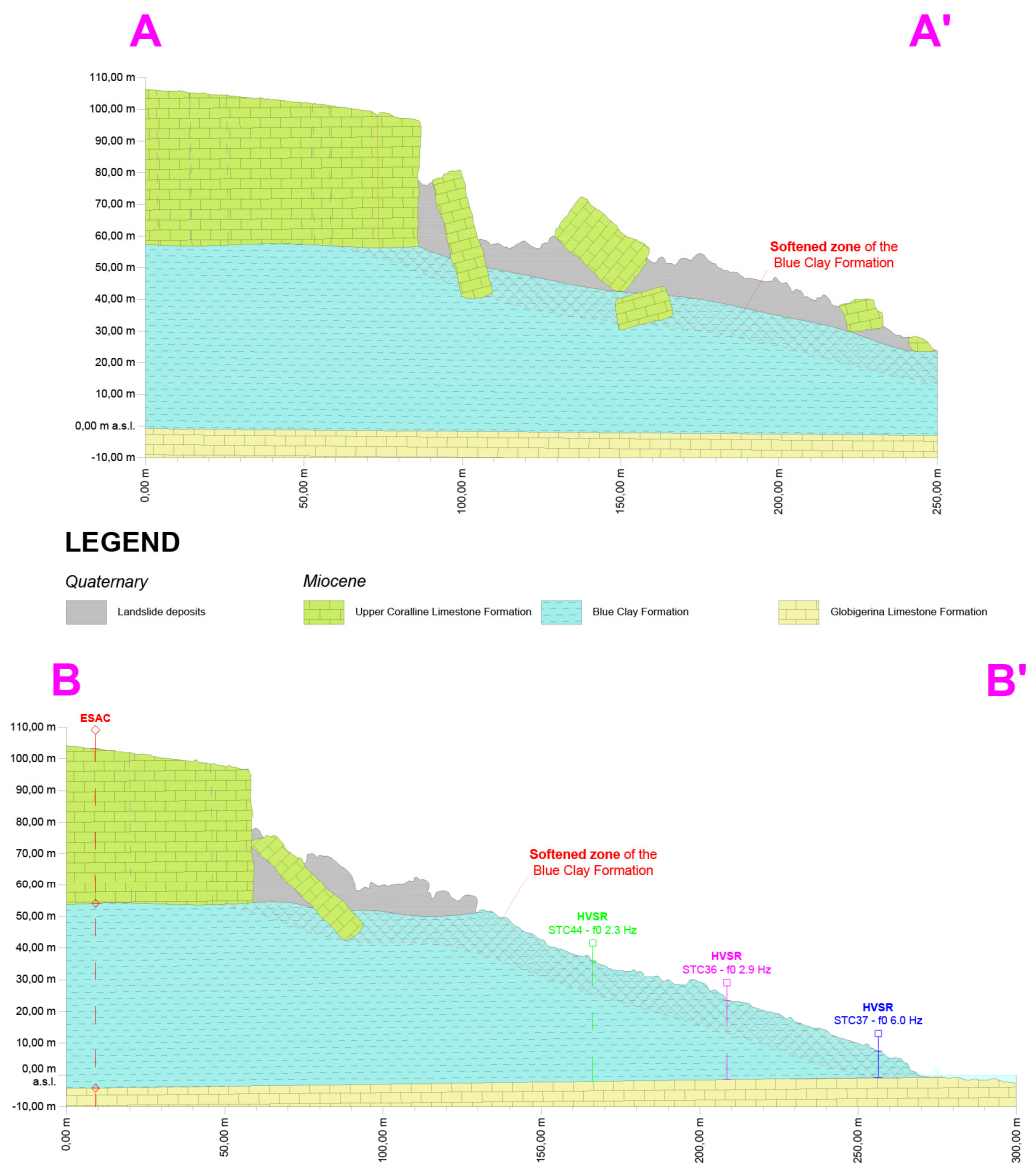


Figure 11. Cross-sections (see Figure 2 for location of traces) of the Sopu promontory.

All these data made it possible to deduce a model that conceptualises the main evolution phases of the expansion process taking place at the promontory (Figure 12, top panel).

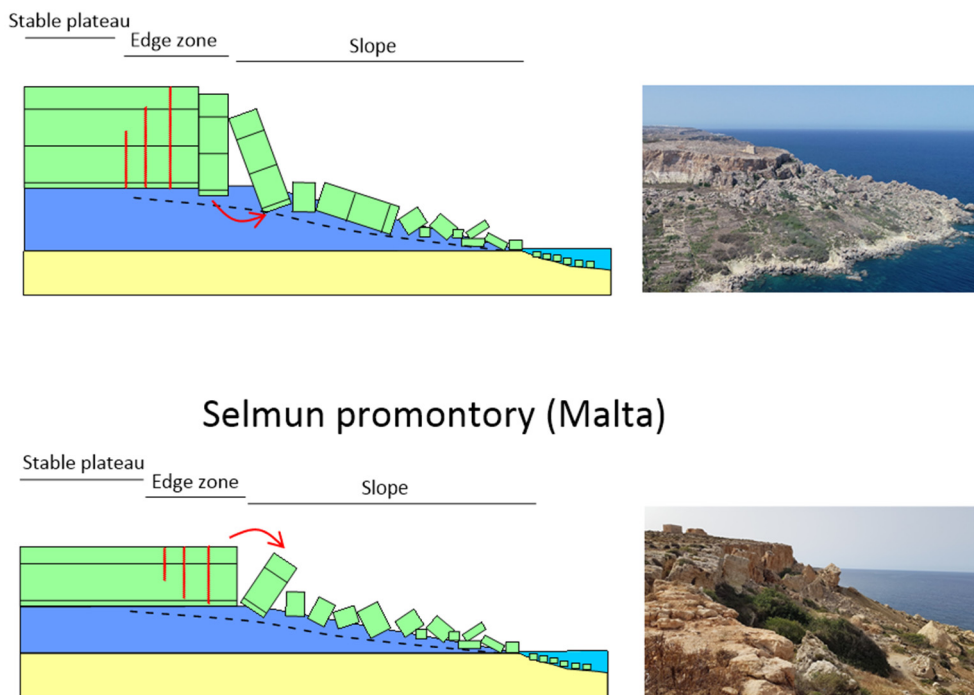


Figure 12. Conceptual models of landslide evolution at Sopus (**top**) and Selmun (**bottom**) promontories.

The dynamics of lateral spreading have been a topic of relevant interest for decades, for the protection of areas exposed to these landslide processes located at the top of the reliefs whose perimeter portions retreat with the ongoing of these phenomena. According to this conceptual model, the thick rigid plateau of UCL produces, with its own weight, the ductile deformation of the underlying BC, and causes an under-sliding which becomes responsible for the generation of tensile stresses within the plateau. Over time, this tensile induces the fracturing of the plateau and the formation of open joints, which tend to propagate towards the surface, or to reopen if in pre-existing, isolating blocks of perimeter rock. These blocks, acquiring kinematic freedom, and finding themselves superimposed on a ductile clay level which gradually erases and undergoes softening, begin to move away from the plateau with mechanisms which, in general, can be toppling or sliding. The former causes the downstream tilt of the rock blocks, while the latter induces their upstream back-tilt.

The literature ([69], [70], [71], and references therein) has already provided various ideas to relate the thickness and width of the rigid plateaus superimposed on more ductile lithologies with the resulting landslide mechanisms. In particular, from what we have learned from the literature, the processes of stress relief are strongly controlled by both width/thickness ratios of the rigid plateau, and from the existence or non-existence of plateau isolation conditions from the adjacent summit plateau. The first factor controls the extent of the overall release of the plateau, and the consequent extension of the gravity-induced instability process from the edge towards the inland part, the effect of which is the overturning of the blocks. The second factor, instead, essentially controls the modes of deformation of the plateau, or the configuration of the concavity of the top profile, in relation to the entity of the insulation of the plateau itself, if compared to the original plateau.

The current influence of the sea for the landslide process evolution can be assumed as negligible. In fact, the sea level is approximately at the BC-GL contact, therefore a seawater intrusion inside the BC layer and their consequent weakening are unlikely. In addition, the direct action of the sea waves on the BC slope and, particularly, on the UCL edge can also be considered unlikely in the light of the present distance. In the past, a higher sea level

may have influenced the slope stability, but the current setting does not provide certain elements to evaluate this contribution.

The present study demonstrates how integrated techniques applied to the near surface can converge on a deformation model of a landslide slope, providing precious elements to support the conceptualization of its failure mechanism. In more detail, the single-station seismic ambient noise measurements allowed the definition of the resonant thicknesses due to their contact with the underlying calcarenites of the LCL. Geoelectrics has constrained the thickness of the softened portion of the clays which, as a result of the expansion process, regulates the deformation rates and causes the disaggregation of the more rigid portion of the overlying calcarenite plateau [72,73]. The ESAC survey made it possible to constrain the thickness of the UCL plateau, a fundamental parameter, as mentioned above, for the evolution of the deformation process. The GPR highlighted the presence of pervasive joints in the rigid plateau which function as kinematic releases to the rock blocks distributed on the perimeter portions of the cliff. Furthermore, the GPR made it possible to demonstrate the persistence of the complex discontinuity network detected on the surface of the stiff plateau.

Particularly significant is the comparison between the geomorphological evolution of the Sopus promontory on the island of Gozo and the Selmun promontory on the island of Malta [4,5,74] in light of the vibrational behaviour observed in the single-station seismic ambient noise measurement analysis results (i.e., HVNR and WAVEPOL). At the Selmun promontory (Figure 12, bottom panel), the overturning of the perimeter blocks of the slope that detached from the cliff in UCL due to the lateral spreading are associated with a clear polarization of the Rayleigh waves orthogonal to the joint direction, as evidenced by the marked polarization and linearity features of the particle motion according to the WAVEPOL analysis results. On the contrary, the back-tilting mechanism affecting the Sopus promontory in its most peripheral portion is only associated with a weak polarization of the f_1 peak in the HVNR analysis observed in a very limited edge sector of the slope, and neither the polarization nor the linearity of the particle motion were observed in the WAVEPOL analysis.

This allows us to hypothesise that the polarization in the Selmun promontory is more directly linked to eigenmodes of the detached rock blocks (“volume controlled” model, sensu Kleinbrod et al. [75]), while in the case of Sopus, the polarized frequencies seem to remain more connected to the stratigraphic structure (“depth controlled” model, sensu Kleinbrod et al. [75]) of the promontory combined with a topographic effect given by the edge of the UCL plateau.

5. Conclusions

The integration of different investigation techniques combined with remote sensing has made it possible to conceptualise the morphodynamic evolution model of the coastal slope of the Sopus promontory on the island of Gozo (Malta). From this analysis, an ongoing process of lateral spreading occurs as a result, which induces the retreat of the slope located at the edge of the rigid calcarenite plateau ascribable to the stiff UCL Formation as it is superimposed on the ductile BC Formation. This retreat is caused by a progressive fracturing of the edge of the stiff plateau, with a propagation mostly from the UCL-BC contact towards the surface which, therefore, becomes particularly visible thanks to GPR techniques. Such a gradual fracturing contributes to the separation of rock blocks by geomechanical joints which, in relation to the thickness/extension ratio of the UCL plateau, tends to undergo a back-tilt, further fragmenting and generating a large layer of debris up to the shoreline. However, the lack of a toppling mechanism, associated with a more marked stress release of the blocks of the stiff summit plateau, leads to the absence of evidence of polarization due to the Rayleigh waves orthogonal to the joints forming at the plateau margin. This is unlike what has been observed in other contexts, such as the Selmun promontory on the island of Malta. The evidence of a different failure mechanism of the rigid UCL plateau between the two sites of Selmun and Sopus, in the same geological

setting, translates into a different output in the interaction between the surface seismic waves and the geostructural elements of the near-surface. This result reveals the sensitivity of the geophysical measurement techniques applied here to detect not only the presence of landslide dynamics in correspondence with a rock slope, but also its different mechanical expression, encouraging further future observations and analyses on this topic.

Author Contributions: In the present paper: S.D. and S.M. coordinated the research; all the authors contributed to carry out the investigations, analyse the data, discuss the results and write the manuscript. All authors have read and agreed to the published version of the manuscript.

Funding: This work was partially supported by the project “Integration of seismic ambient noise measurements and engineering geological surveys for the purposes of local seismic response study” (prot. n. AR21916B7BB6A787; P.I. R. Iannucci) of 2019 Research Initiation Projects of Sapienza University of Rome. The University of Malta team was supported by the project Multi-disciplinary monitoring system for a resilient management of coastal areas (REMACO) funded by the INTERREG V A –Italy-Malta Capitalization Programme (local P.I., S. D’Amico).

Data Availability Statement: Analysed data can be provided upon request.

Acknowledgments: The activities of R. Iannucci were mainly performed during his postdoctoral research fellowship at the Department of Earth Sciences of Sapienza University of Rome.

Conflicts of Interest: The authors declare no conflicts of interest.

References

- Cruden, D.M.; Varnes, D.J. Landslide types and processes. In *Landslides. Investigation and Mitigation*; Turner, A.K., Shuster, R.L., Eds.; Special Report 247; Transportation Research Board: Washington, DC, USA, 1996; pp. 36–75.
- Hungr, O.; Leroueil, S.; Picarelli, L. The Varnes classification of landslide types, an update. *Landslides* **2014**, *11*, 167–194. [[CrossRef](#)]
- Chigira, M. Long-term gravitational deformation of rocks by mass rock creep. *Eng. Geol.* **1992**, *32*, 157–184. [[CrossRef](#)]
- Iannucci, R.; Martino, S.; Paciello, A.; D’Amico, S.; Galea, P. Engineering geological zonation of a complex landslide system through seismic ambient noise measurements at the Selmun Promontory (Malta). *Geophys. J. Int.* **2018**, *213*, 1146–1161. [[CrossRef](#)]
- Iannucci, R.; Martino, S.; Paciello, A.; D’Amico, S.; Galea, P. Investigation of cliff instability at Ghajn Hadid Tower (Selmun Promontory, Malta) by integrated passive seismic techniques. *J. Seismol.* **2020**, *24*, 897–916. [[CrossRef](#)]
- Martino, S.; Cercato, M.; Della Seta, M.; Esposito, C.; Hailemikael, S.; Iannucci, R.; Martini, G.; Paciello, A.; Mugnozza, G.S.; Seneca, D.; et al. Relevance of rock slope deformations in local seismic response and microzonation: Insights from the Accumoli case-study (central Apennines, Italy). *Eng. Geol.* **2020**, *266*, 105427. [[CrossRef](#)]
- Bozzano, F.; Bretschneider, A.; Esposito, C.; Martino, S.; Prestinanzi, A.; Scarascia Mugnozza, G. Lateral spreading processes in mountain ranges: Insights from an analogue modelling experiment. *Tectonophysics* **2013**, *605*, 88–95. [[CrossRef](#)]
- Discenza, M.E.; Martino, S.; Bretschneider, A.; Scarascia Mugnozza, G. Influence of joints on creep processes involving rock masses: Results from physical-analogue laboratory tests. *Int. J. Rock Mech. Min. Sci.* **2020**, *128*, 104261. [[CrossRef](#)]
- Mantovani, M.; Devoto, S.; Forte, E.; Mocnik, A.; Pasuto, A.; Piacentini, D.; Soldati, M. A multidisciplinary approach for rock spreading and block sliding investigation in the north-western coast of Malta. *Landslides* **2013**, *10*, 611–622. [[CrossRef](#)]
- Martino, S.; Mazzanti, P. Integrating geomechanical surveys and remote sensing for sea cliff slope stability analysis: The Mt. Pucci case study (Italy). *Nat. Hazards Earth Syst. Sci.* **2014**, *14*, 831–848. [[CrossRef](#)]
- Illies, J.H. Graben formation—The Maltese Islands—A case history. *Tectonophysics* **1981**, *73*, 151–168. [[CrossRef](#)]
- Pedley, M. The Calabrian Stage, Pleistocene highstand in Malta: A new marker for unravelling the Late Neogene and Quaternary history of the islands. *J. Geol. Soc.* **2011**, *168*, 913–926. [[CrossRef](#)]
- Galve, J.P.; Tonelli, C.; Gutiérrez, F.; Lugli, S.; Vescogni, A.; Soldati, M. New insights into the genesis of the Miocene collapse structures of the island of Gozo (Malta, central Mediterranean Sea). *J. Geol. Soc.* **2015**, *172*, 336–348. [[CrossRef](#)]
- Gardiner, W.; Grasso, M.; Sedgely, D. Plio-pleistocene fault movement as evidence for mega-block kinematics within the Hyblean—Malta Plateau, Central Mediterranean. *J. Geodyn.* **1995**, *19*, 35–51. [[CrossRef](#)]
- Jongsma, D.; van Hinte, J.E.; Woodside, J.M. Geologic structure and neotectonics of the North African Continental Margin south of Sicily. *Mar. Pet. Geol.* **1985**, *2*, 156–179. [[CrossRef](#)]
- Alexander, D. A review of the physical geography of Malta and its significance for tectonic geomorphology. *Quat. Sci. Reviews* **1988**, *7*, 41–53. [[CrossRef](#)]
- Oil Exploration Directorate. *Geological Map of the Maltese Islands*; Office of the Prime Minister: Valletta, Malta, 1993.
- Pedley, H.M.; Clarke, M.H.; Galea, P. *Limestone Isles in a Crystal Sea: The Geology of the Maltese Islands*; Publishers Enterprises Group: Valletta, Malta, 2002.
- Baldassini, N.; Di Stefano, A. Stratigraphic features of the Maltese archipelago: A synthesis. *Nat. Hazards* **2017**, *86*, 203–231. [[CrossRef](#)]

20. Scerri, S. Sedimentary evolution and resultant geological landscapes. In *Landscapes and Landforms of the Maltese Islands*; Gauci, R., Schembri, J., Eds.; World Geomorphological Landscapes; Springer: Cham, Switzerland, 2019; pp. 31–47.
21. Prampolini, M.; Gauci, C.; Micallef, A.S.; Selmi, L.; Vandelli, V.; Soldati, M. Geomorphology of the north-eastern coast of Gozo (Malta, Mediterranean Sea). *J. Maps* **2018**, *14*, 402–410. [[CrossRef](#)]
22. Rizzo, A.; Vandelli, V.; Buhagiar, G.; Micallef, A.S.; Soldati, M. Coastal Vulnerability Assessment along the North-Eastern Sector of Gozo Island (Malta, Mediterranean Sea). *Water* **2020**, *12*, 1405. [[CrossRef](#)]
23. Soldati, M. Deep-seated gravitational slope deformation. In *Encyclopedia of Geomorphology*; Goudie, A., Ed.; Routledge: London, UK, 2004; pp. 226–228.
24. Pasuto, A.; Soldati, M.; Tecca, P.R. Lateral Spread: From Rock to Soil Spreading. In *Treatise on Geomorphology*, 2nd ed.; Shroder, J.F., Ed.; Academic Press: Cambridge, MA, USA, 2022; Volume 5, pp. 169–182.
25. Soldati, M.; Barrows, T.T.; Prampolini, M.; Fifield, K.L. Cosmogenic exposure dating constraints for coastal landslide evolution on the Island of Malta (Mediterranean Sea). *J. Coast. Conserv.* **2018**, *22*, 831–844. [[CrossRef](#)]
26. Hoek, E.; Bray, J.W. *Rock Slope Engineering*; Taylor & Francis: London, UK, 1981.
27. Hutchinson, J.N. General report: Morphological and geotechnical parameters of landslides in relation to geology and hydrogeology. In Proceedings of the 5th International Symposium on Landslides, Lausanne, Balkema, Rotterdam, The Netherlands, 10–15 July 1988; pp. 3–35.
28. Furlani, S.; Antonioli, F.; Biolchi, S.; Gambin, T.; Gauci, R.; Presti, V.L.; Anzidei, M.; Devoto, S.; Palombo, M.; Sulli, A. Holocene sea level change in Malta. *Quat. Int.* **2013**, *288*, 146–157. [[CrossRef](#)]
29. ISRM Suggested methods for the quantitative description of discontinuities in rock masses. *Int. J. Rock Mech. Min. Sci. Geomech. Abstr.* **1978**, *15*, 319–368.
30. Colica, E.; Micallef, A.; D’Amico, S.; Cassar, L.F.; Galdies, C. Investigating the use of UAV systems for photogrammetric applications: A case study of Ramla Bay (Gozo, Malta). *Xjenza* **2017**, *5*, 125–131.
31. Colica, E.; D’Amico, S.; Iannucci, R.; Martino, S.; Gauci, A.; Galone, L.; Galea, P.; Paciello, A. Using unmanned aerial vehicle photogrammetry for digital geological surveys: Case study of Selmun promontory, northern of Malta. *Environ. Earth Sci.* **2021**, *80*, 551. [[CrossRef](#)]
32. Colica, E.; Galone, L.; D’Amico, S.; Gauci, A.; Iannucci, R.; Martino, S.; Pistillo, D.; Iregbeyen, P.; Valentino, G. Evaluating characteristics of an active coastal spreading area combining geophysical data with satellite, aerial, and unmanned aerial vehicles images. *Remote Sens.* **2023**, *15*, 1465. [[CrossRef](#)]
33. Furlani, S.; Antonioli, F.; Colica, E.; D’Amico, S.; Devoto, S.; Grego, P.; Gambin, T. Sea caves and other landforms of the coastal scenery on Gozo Island (Malta): Inventory and new data on their formation. *Geosciences* **2023**, *13*, 164. [[CrossRef](#)]
34. El Gamal, A.; Eltoukhy, H. CMOS image sensors. *IEEE Circuits Devices Mag.* **2005**, *21*, 6–20. [[CrossRef](#)]
35. Agisoft Metashape Documentation. Agisoft Metashape User Manual, Professional Edition, Version 2.0. Available online: https://www.agisoft.com/pdf/metashape-pro_2_0_en.pdf (accessed on 24 November 2023).
36. Daniels, D.J. Surface-penetrating radar. *Electron. Commun. Eng. J.* **1996**, *8*, 165–182. [[CrossRef](#)]
37. Loke, M.H. Electrical imaging surveys for environmental and engineering studies. A practical guide to 2-D and 3-D surveys. *A Pract. Guide* **1999**, *2*, 70.
38. Loke, M.H.; Dahlin, T. A comparison of the Gauss–Newton and Quasi-Newton methods in resistivity imaging inversion. *J. Appl. Geophys.* **2002**, *49*, 149–162. [[CrossRef](#)]
39. Loke, M.H.; Acworth, I.; Dahlin, T. A comparison of smooth and blocky inversion methods in 2D electrical imaging surveys. *Explor. Geophys.* **2003**, *34*, 182–187. [[CrossRef](#)]
40. Nogoshi, M.; Igarashi, T. On the propagation characteristics of microtremors. *J. Seism. Soc. Japan.* **1970**, *23*, 264–280. (In Japanese with English abstract)
41. Nogoshi, M.; Igarashi, T. On the amplitude characteristics of microtremors. *J. Seism. Soc. Japan.* **1971**, *24*, 24–40. (In Japanese with English abstract)
42. Nakamura, Y. A method for dynamic characteristics estimation of subsurface using microtremor on the ground surface. *Q. Rep. Railw. Tech. Res. Inst. (RTRI)* **1989**, *30*, 25–33.
43. Bour, M.; Fouissac, D.; Dominique, P.; Martin, C. On the use of microtremor recordings in seismic microzonation. *Soil Dyn. Earthq. Eng.* **1998**, *17*, 465–474. [[CrossRef](#)]
44. Haghshenas, E.; Bard, P.-Y.; Theodulidis, N. SESAME WP04 Team Empirical evaluation of microtremor H/V spectral ratio. *Bull. Earthq. Eng.* **2008**, *6*, 75–108. [[CrossRef](#)]
45. Panzera, F.; D’Amico, S.; Lotteri, A.; Galea, P.; Lombardo, G. Seismic site response of unstable steep slope using noise measurements: The case study of Xemxija Bay area, Malta. *Nat. Hazards Earth Syst. Sci.* **2012**, *12*, 3421–3431. [[CrossRef](#)]
46. Galea, P.; D’Amico, S.; Farrugia, D. Dynamic characteristics of an active coastal spreading area using ambient noise measurements—Anchor Bay, Malta. *Geophys. J. Int.* **2014**, *199*, 1166–1175. [[CrossRef](#)]
47. Galone, L.; D’Amico, S.; Colica, E.; Iregbeyen, P.; Galea, P.; Rivero, L.; Villani, F. Assessing Shallow Soft Deposits through Near-Surface Geophysics and UAV-SfM: Application in Pocket Beaches Environments. *Remote Sens.* **2023**, *16*, 40. [[CrossRef](#)]
48. Wathelet, M.; Chatelain, J.L.; Cornou, C.; Di Giulio, G.; Guillier, B.; Ohrnberger, M.; Savvaidis, A. Geopsy: A user-friendly open-source tool set for ambient vibration processing. *Seismol. Res. Lett.* **2020**, *91*, 1878–1889. [[CrossRef](#)]

49. Konno, K.; Ohmachi, T. Ground-motion characteristics estimated from spectral ratio between horizontal and vertical components of microtremor. *Bull. Seismol. Soc. Am.* **1998**, *88*, 228–241. [[CrossRef](#)]
50. Vidale, J.E. Complex Polarization Analysis of Particle Motion. *Bull. Seismol. Soc. Am.* **1986**, *76*, 1393–1405.
51. Burjánek, J.; Gassner-Stamm, G.; Poggi, V.; Moore, J.R.; Fäh, D. Ambient vibration analysis of an unstable mountain slope. *Geophys. J. Int.* **2010**, *180*, 820–828. [[CrossRef](#)]
52. Burjánek, J.; Moore, J.R.; Molina, F.X.Y.; Fäh, D. Instrumental evidence of normal mode rock slope vibration. *Geophys. J. Int.* **2012**, *188*, 559–569. [[CrossRef](#)]
53. Panzera, F.; D’Amico, S.; Galea, P.; Lombardo, G.; Gallipoli, M.R.; Pace, S. Geophysical measurements for site response investigation: Preliminary results on the island of Malta. *Boll. Geofis. Teor. Appl.* **2013**, *54*, 111–128.
54. Vella, A.; Galea, P.; D’Amico, S. Site frequency response characterisation of the Maltese islands based on ambient noise H/V ratios. *Eng. Geol.* **2013**, *163*, 89–100. [[CrossRef](#)]
55. Farrugia, D.; Paolucci, E.; D’Amico, S.; Galea, P. Inversion of surface wave data for subsurface shear wave velocity profiles characterized by a thick buried low-velocity layer. *Geophys. J. Int.* **2016**, *206*, 1221–1231. [[CrossRef](#)]
56. Farrugia, D.; Galea, P.; D’Amico, S.; Paolucci, E. Sensitivity of ground motion parameters to local shear-wave velocity models: The case of buried low-velocity layers. *Soil Dyn. Earthq. Eng.* **2017**, *100*, 196–205. [[CrossRef](#)]
57. Pischiutta, M.; Villani, F.; D’Amico, S.; Vassallo, M.; Cara, F.; Di Naccio, D.; Farrugia, D.; Di Giulio, G.; Amoroso, S.; Cantore, L.; et al. Results from shallow geophysical investigations in the northwestern sector of the island of Malta. *Phys. Chem. Earth* **2017**, *98*, 41–48. [[CrossRef](#)]
58. Castellaro, S.; Mulargia, F. The effect of velocity inversions on H/V. *Pure Appl. Geophys.* **2009**, *166*, 567–592. [[CrossRef](#)]
59. Foti, S.; Lai, C.G.; Rix, G.J.; Strobbia, C. *Surface Wave Methods for Near-Surface Site Characterization*; CRC Press: Boca Raton, FL, USA, 2015.
60. Yamanaka, H.; Ishida, H. Application of genetic algorithms to an inversion of surface-wave dispersion data. *Bull. Seismol. Soc. Am.* **1996**, *86*, 436–444. [[CrossRef](#)]
61. Picozzi, M.; Albarello, D. Combining genetic and linearized algorithms for a two-step joint inversion of Rayleigh wave dispersion and H/V spectral ratio curves. *Geophys. J. Int.* **2007**, *169*, 189–200. [[CrossRef](#)]
62. Scherbaum, F.; Hinzen, K.-G.; Ohrnberger, M. Determination of shallow shear wave velocity profiles in the Cologne, Germany area using ambient vibrations. *Geophys. J. Int.* **2003**, *152*, 597–612. [[CrossRef](#)]
63. Arai, H.; Tokimatsu, K. S-wave velocity profiling by inversion of microtremor H/V spectrum. *Bull. Seismol. Soc. Am.* **2004**, *94*, 53–63. [[CrossRef](#)]
64. Parolai, S.; Picozzi, M.; Richwalski, S.M.; Milkereit, C. Joint inversion of phase velocity dispersion and H/V ratio curves from seismic noise recordings using a genetic algorithm, considering higher modes. *Geophys. Res. Lett.* **2005**, *32*, L01303. [[CrossRef](#)]
65. Asten, M.W.; Askan, A.; Ekincioglu, E.E.; Sisman, F.N.; Ugurhan, B. Site characterisation in north-western Turkey based on SPAC and HVSR analysis of microtremor noise. *Explor. Geophys.* **2014**, *45*, 74–85. [[CrossRef](#)]
66. Shabani, E.; Cornou, C.; Haghshenas, E.; Wathelet, M.; Bard, P.-Y.; Mirzaei, N.; Eskandari-Ghadi, M. Estimating shear-waves velocity structure by using array methods (FK and SPAC) and inversion of ellipticity curves at a site in south of Tehran. In Proceedings of the 14th World Conference on Earthquake Engineering, Beijing, China, 12–17 October 2008.
67. Picozzi, M.; Strollo, A.; Parolai, S.; Durukal, E.; Ozel, O.; Karabulut, S.; Zschau, J.; Erdik, M. Site characterization by seismic noise in Istanbul, Turkey. *Soil Dyn. Earthq. Eng.* **2009**, *29*, 469–482.
68. Albarello, D.; Cesi, C.; Eulilli, V.; Guerrini, F.; Lunedei, E.; Paolucci, E.; Pileggi, D.; Puzzilli, L.M. The contribution of the ambient vibration prospecting in seismic microzoning: An example from the area damaged by the April 6, 2009 L’Aquila (Italy) earthquake. *Boll. Geofis. Teor. Appl.* **2011**, *52*, 513–538.
69. Bozzano, F.; Floris, M.; Gaeta, M.; Martino, S.; Scarascia Mugnozza, G. Assetto geologico ed evoluzione per frana di rupi vulcaniche nel Lazio Settentrionale. *Boll. Soc. Geol. It.* **2005**, *124*, 413.
70. Casagli, N. Fenomeni di instabilità in ammassi rocciosi sovrastanti un substrato deformabile: Analisi di alcuni esempi nell’Appennino settentrionale. *Geol. Romana* **1994**, *30*, 607–618.
71. Mantovani, M.; Bossi, G.; Dykes, A.P.; Pasuto, A.; Soldati, M.; Devoto, S. Coupling long-term GNSS monitoring and numerical modelling of lateral spreading for hazard assessment purposes. *Eng. Geol.* **2022**, *296*, 106466. [[CrossRef](#)]
72. Tommasi, P.; Pellegrini, P.; Boldini, D.; Ribacchi, R. Influence of rainfall on hydraulic conditions and movement rates in the Orvieto hill (central Italy). *Can. Geotech. J.* **2006**, *43*, 70–86. [[CrossRef](#)]
73. Bozzano, F.; Bretschneider, A.; Martino, S. Stress–strain history from the geological evolution of the Orvieto and Radicofani cliff slopes (Italy). *Landslides* **2008**, *5*, 351–366. [[CrossRef](#)]
74. Iannucci, R.; Martino, S.; Paciello, A.; D’Amico, S. Rock mass characterization coupled with seismic noise measurements to analyze the unstable cliff slope of the Selmun Promontory (Malta). *Procedia Eng.* **2017**, *191*, 263–269. [[CrossRef](#)]
75. Kleinbrod, U.; Burjánek, J.; Fäh, D. Ambient vibration classification of unstable rock slopes: A systematic approach. *Eng. Geol.* **2019**, *249*, 198–217. [[CrossRef](#)]

Disclaimer/Publisher’s Note: The statements, opinions and data contained in all publications are solely those of the individual author(s) and contributor(s) and not of MDPI and/or the editor(s). MDPI and/or the editor(s) disclaim responsibility for any injury to people or property resulting from any ideas, methods, instructions or products referred to in the content.